

Effect of carbon content on microstructural characteristics of the hypereutectic Fe–Cr–C claddings

Chia-Ming Chang^a, Chi-Ming Lin^a, Chih-Chun Hsieh^a, Jie-Hao Chen^a,
Chih-Ming Fan^b, Weite Wu^{a,*}

^a Department of Materials Science and Engineering, National Chung Hsing University, 250 Kuo-Kuang Rd., Taichung, Taiwan

^b Kuang Tai Metal Industrial Co., Ltd., 8 Lu-Ke Third Rd., Lujhu Township, Kaohsiung, Taiwan

ARTICLE INFO

Article history:

Received 3 November 2008

Received in revised form 29 April 2009

Accepted 28 May 2009

Keywords:

Carbide

Welding

Microstructure

Hardness

ABSTRACT

The hypereutectic Fe–Cr–C claddings with different C contents were deposited on ASTM A36 steel substrates by flux cored arc welding (FCAW) to investigate that the effect of C content on microstructural characteristics. The results showed that the microstructure of hypereutectic Fe–Cr–C claddings consisted of primary proeutectic (Cr,Fe)₇C₃ and the austenite plus (Cr,Fe)₇C₃ eutectic. Proeutectic carbides undergone to several microstructural changes in response to higher carbon content in the cladding. The morphologies of proeutectic (Cr,Fe)₇C₃ carbides changed from blade-like to rod-like with hexagonal cross section. The amounts of proeutectic (Cr,Fe)₇C₃ carbides increased with increase of the C contents. The nucleation sites of proeutectic (Cr,Fe)₇C₃ carbides increased under high undercooling condition. Hence, the latent heat of solidification can be released by formed proeutectic (Cr,Fe)₇C₃ carbides and then the growth of proeutectic (Cr,Fe)₇C₃ carbides were suppressed. Consequently, it showed a maximum hardness value (about HRC 62) when the amount of proeutectic (Cr,Fe)₇C₃ carbides exceeded 86%.

© 2009 Elsevier B.V. All rights reserved.

1. Introduction

Fe–Cr–C alloys are used in severe abrasive conditions, so the superior abrasion resistance is necessary. The excellent abrasive wear resistance results from high volume fraction of carbides and the toughness of the matrix also contribute to the wear resistance [1]. The investigations of Fe–Cr–C alloy microstructures have shown that these types of materials have hypoeutectic, eutectic, and hypereutectic structures [2]. M₇C₃ primary carbides form in large amounts at higher carbon concentration. The coating microstructure consists of primarily solidified chromium-carbides of the M₇C₃-type, which are embedded in the eutectic [3,4]. Earlier research on Fe–Cr–C alloys produced with conventional techniques has revealed the formation of microstructures comprising α-ferrite and complex carbides, such as M₃C, M₇C₃ and M₂₃C₆, depending on the alloy composition [4,5]. M₇C₃ primary carbides formed when the carbon content is 2–5 wt.% and chromium content is 18–30 wt.%. This kind of hard material can be represented by high chromium white cast iron which has high hardness M₇C₃ (about 1600 Hv) [6–8]. Cr₇C₃ is well known for its excel-

lent combination of high hardness, excellent wear resistance as well as good corrosion and oxidation resistance, so it has been widely used as the reinforcing phase in the composite coatings [9–12].

Most researches focus on that the solidification behavior, microstructural characteristics (such as hypoeutectic, eutectic, and hypereutectic), and mechanical properties of Fe–Cr–C system. However, there are few investigations about morphology of primary carbide in Fe–Cr–C system. Therefore, the relationship between the morphology of primary carbide and the carbon content of hypereutectic Fe–Cr–C claddings was investigated in this study.

2. Experimental procedures

The base metals (100 mm × 80 mm × 10 mm) for the welding surface were prepared from ASTM A36 steel plates. Before welding, these specimens were ground and cleaned with acetone. In order to get the claddings with different carbon contents and their chemical composition must fall down in hypereutectic area, different amounts of graphite (7, 10 and 13 wt.%), the constant chromium powder (40 wt.%), and ferrosilicon (2 wt.%), ferromanganese (5 wt.%) were added into flux cored wire. The addition of ferrosilicon and ferromanganese were used to reduce the oxygen of claddings.

Bead-on-plate with oscillate flux cored arc welding was utilized to deposited the claddings. Fig. 1 shows the schematic diagram of the welding method. Table 1 presents the range of welding conditions used in this research.

* Corresponding author.

E-mail address: wwu@nchu.edu.tw (W. Wu).

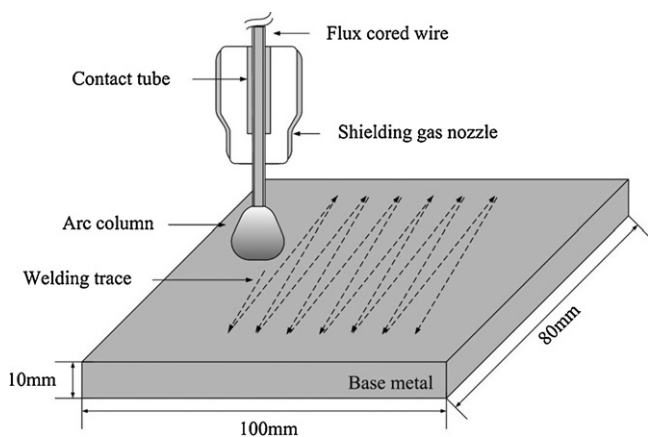


Fig. 1. The schematic diagram of flux cored arc welding for the cladding.

Table 1

FCAW condition.

Parameter	Value
Wire diameter	2.8 mm
Voltage	33 V
Current	350 A
Travel speed	200 mm min ⁻¹
Oscillate speed	300 mm min ⁻¹
Contact tube to work distance	50 mm
Cladding thickness	5 mm

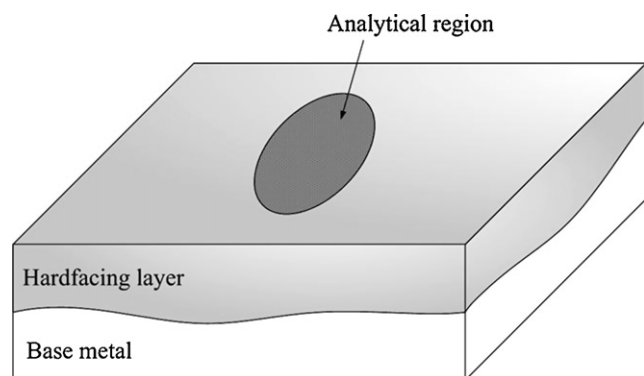


Fig. 2. The schematic diagram of analytic position using OES and Rockwell hardness tester.

An optical emission spectrum (OES) was utilized to analyze the chemical composition of the claddings, which was shown in Table 2. The hardness values HRC were taken on the top surface of the claddings. Fig. 2 shows the analytic position using OES and Rock hardness tester. The microstructures of the claddings were characterized by optical and field emission scanning electron microscope. The amounts, size and number of proeutectic carbides were measured by image analysis software.

Table 2

Chemical compositions and amounts, size and number of proeutectic (Cr,Fe)₇C₃ carbides for claddings and base metal.

Claddings	Composition (wt.%)					F_{carbide} (%)	D_{carbide} (μm)	N_{carbide} (# mm ⁻²)
	C	Si	Mn	Cr	Fe			
Base metal (A36)	0.18	0.15	0.55	0.09	bal.	–	–	–
Cladding A	3.73	2.28	2.33	26.70	bal.	33.81	59.00	565
Cladding B	4.21	2.00	2.26	27.08	bal.	61.19	33.39	1004
Cladding C	4.85	1.96	2.28	27.31	bal.	86.14	13.53	3758

F_{carbide} : amount of primary carbides, D_{carbide} : size of primary carbides, and N_{carbide} : number of primary carbides per unit area.

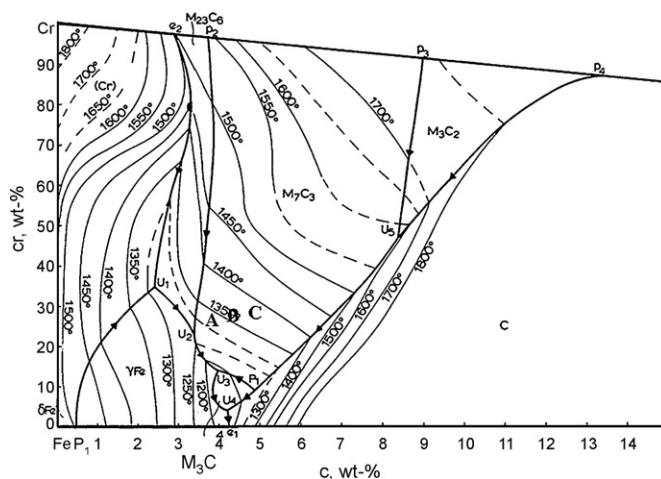


Fig. 3. Liquidus projection for the Fe–Cr–C ternary system.

3. Results and discussion

In this study, the claddings with three carbon contents were deposited on ASTM A36 steel substrates by flux cored arc welding. Their chemical compositions were analyzed by OES. Fig. 3 was the liquidus projection of the iron corner of the Fe–Cr–C ternary system [13–15], with points A, B and C corresponding to the alloys listed in Table 2. According to Fig. 3, it was understood that the primary phases were M₇C₃ in these claddings. When these claddings started to solidify, the proeutectic (Cr,Fe)₇C₃ carbides appeared first. After that, the eutectic structure formed around the proeutectic (Cr,Fe)₇C₃ grain boundary, as shown in Fig. 4. Therefore, these claddings were hypereutectic structure with proeutectic (Cr,Fe)₇C₃ and austenite plus (Cr,Fe)₇C₃ eutectic. According to previous researches [16–19], the morphology of M₇C₃ carbides included rod-like and blade-like shape in Fe–Cr–C systems. The proeutectic (Cr,Fe)₇C₃ carbides and austenite plus (Cr,Fe)₇C₃ eutectic were obtained in these claddings.

According to Fig. 4, the amounts, size and number of primary carbides were measured by image analysis software, which were shown in Table 2. The amounts of proeutectic (Cr,Fe)₇C₃ carbides in claddings increased from 33.81 to 86.14% when carbon content increased from 3.73 to 4.85 wt.%. For an off-eutectic composition, the alloy liquidus was much higher than the eutectic temperature. Thus the corresponding primary phase was highly undercooling and tends to grow faster than the eutectic [1]. Comparison among Fig. 5a–c showed that increasing the carbon content promotes the formation of proeutectic (Cr,Fe)₇C₃ carbide. The carbon addition lowered the eutectic temperature for the Fe–Cr–C alloy [20]. The lower eutectic temperature caused the amount of eutectic structure decreasing. Therefore, the increase in carbon content caused that the fraction of proeu-

tectic $(\text{Cr,Fe})_7\text{C}_3$ carbides increased and the eutectic structure decreased.

From Table 2, in alloys A, B and C, the size of proeutectic $(\text{Cr,Fe})_7\text{C}_3$ carbides decreased from 59.00 to 13.53 μm when the carbon content increased from 3.73 to 4.85 wt.%. This phenomenon could be explained by the fact that the nucleation rate was higher than growth rate when the carbon content increased. From Table 2, the number of carbides increasing per mm^2 increased from 565 to 3758 when the carbon content increased from 3.73 to 4.85 wt.%. Therefore, the carbon addition led into the nucleation rate of proeutectic $(\text{Cr,Fe})_7\text{C}_3$ carbide increasing. During solidification, the formation of proeutectic $(\text{Cr,Fe})_7\text{C}_3$ carbide released the latent heat caused the reduction of undercooling [20]. The more proeutectic $(\text{Cr,Fe})_7\text{C}_3$ carbides formed, the more solidification latent heat was released. The undercooling of solid–liquid interface decreased because the solidification latent heat was released. The growth of proeutectic $(\text{Cr,Fe})_7\text{C}_3$ carbides was suppressed as the undercooling of solid–liquid interface decreased. Consequently, the size of proeutectic $(\text{Cr,Fe})_7\text{C}_3$ carbides decreased when the carbon content of claddings increased.

In Fig. 4, the morphology of proeutectic $(\text{Cr,Fe})_7\text{C}_3$ carbides transitioned from blade-like to rod-like while carbon content increased. The solidification morphology and its growth pattern of cladding metal were controlled by the thermal conditions in the weld pool. The formation and growth of the proeutectic $(\text{Cr,Fe})_7\text{C}_3$ carbides during solidification occurred with their long axes parallel to the direction of the heat flow. In lower carbon content, the nuclei sites of proeutectic $(\text{Cr,Fe})_7\text{C}_3$ carbides were fewer and the growth direction of primary carbide was random. The proeutectic $(\text{Cr,Fe})_7\text{C}_3$

carbide rods appeared as blade-like shape when its axis was perpendicular to the viewing surface. With the carbon content of claddings increasing, the nuclei sites of proeutectic $(\text{Cr,Fe})_7\text{C}_3$ carbides increased. The $(\text{Cr,Fe})_7\text{C}_3$ carbide rods appeared as blade-like shape when its axis was perpendicular to the viewing surface. Therefore, the morphology of proeutectic $(\text{Cr,Fe})_7\text{C}_3$ carbides transitioned from blade-like to rod-like as the carbon content of claddings increased.

The schematic diagram of microstructural transition was illustrated in Fig. 6. For a given Cr content, as the higher C content of hypereutectic Fe–Cr–C claddings promoted the formation of proeutectic $(\text{Cr,Fe})_7\text{C}_3$ carbides, which caused the amounts and number of proeutectic $(\text{Cr,Fe})_7\text{C}_3$ carbides increasing. Besides, the formation of proeutectic $(\text{Cr,Fe})_7\text{C}_3$ released latent heat that led into the decrease in undercooling of solid–liquid interface, which caused that the growth rate of proeutectic $(\text{Cr,Fe})_7\text{C}_3$ carbides decreased. Hence, the size of proeutectic $(\text{Cr,Fe})_7\text{C}_3$ carbides decreased with the C content increasing.

Fig. 7 showed the results of hardness measured from the cladding for different carbon contents. The maximum hardness value was obtained in the cladding surface of specimen C. The highest hardness in the surface of cladding C was associated with great amount of proeutectic $(\text{Cr,Fe})_7\text{C}_3$, which favored by high carbon amount when compared with the other claddings. Additionally, the hardness was in inverse proportion to the size of particle. Therefore, the smallest proeutectic $(\text{Cr,Fe})_7\text{C}_3$ also caused the increase in hardness.

In general, the two constituents of wear resistant materials serve different functions. Hard proeutectic $(\text{Cr,Fe})_7\text{C}_3$ provides

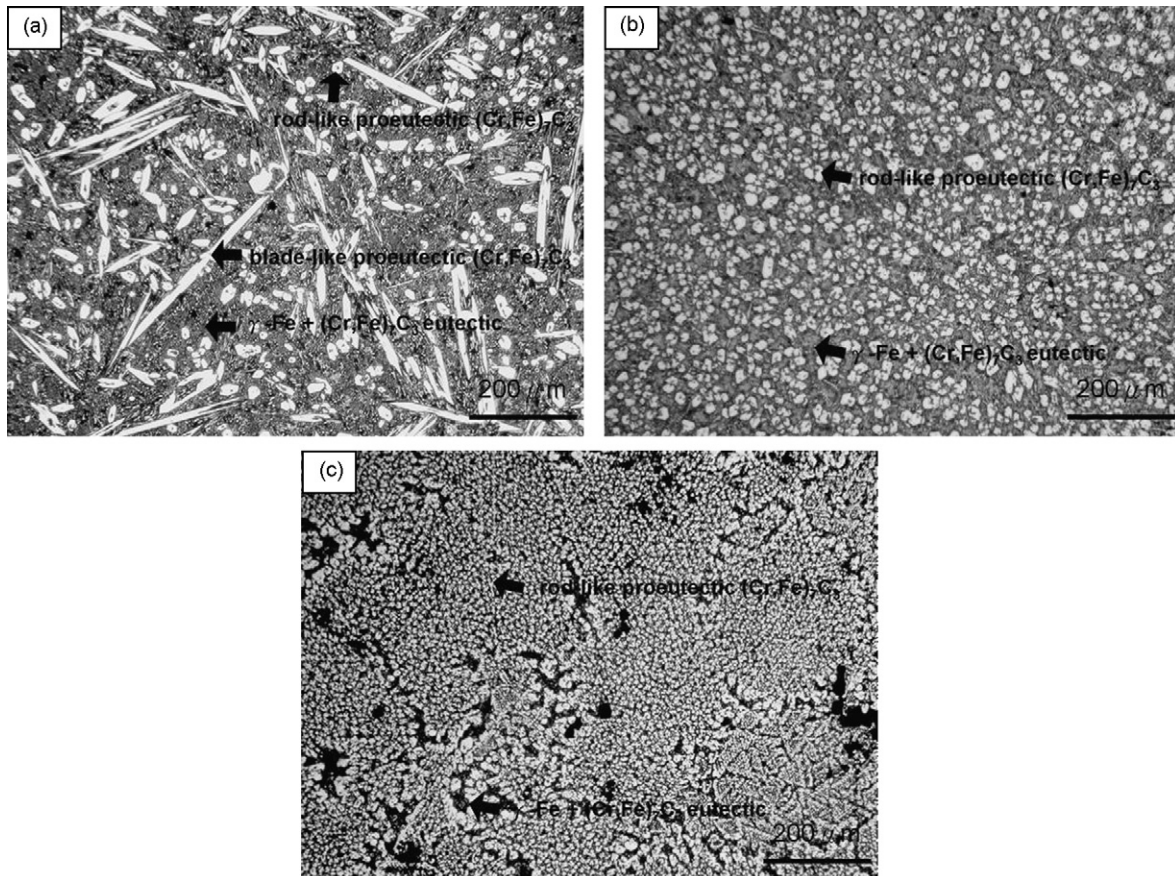


Fig. 4. OM photograph of hypereutectic Fe–Cr–C claddings with different C contents: (a) 3.73 wt.% C; (b) 4.21 wt.% C; (c) 4.85 wt.% C.

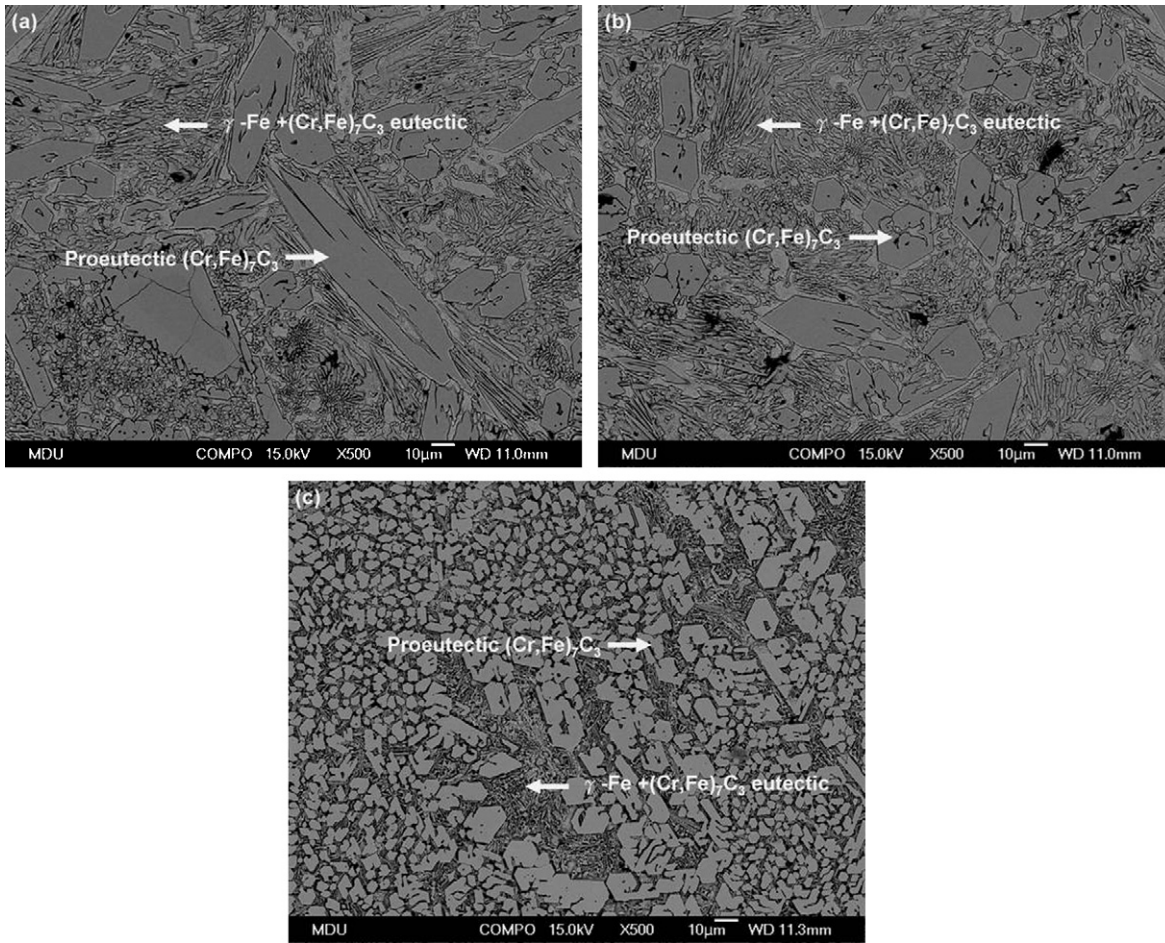


Fig. 5. SEM photography of hypereutectic Fe–Cr–C claddings with different C contents: (a) 3.73 wt.% C; (b) 4.21 wt.% C; (c) 4.85 wt.% C.

to impede wear by grooving or indenting mineral particles. Tough austenite is meant to provide sufficient toughness and support hard carbides. Both properties depend on the amount, size and distribution of hard particles as well as on the hardness and fracture toughness of both constituents and the bond

between them. The dense and fine proeutectic carbides will prevent from the selective abrasion of austenitic matrix. Consequently, the wear resistance and hardness can be improved by large amounts of proeutectic carbides attributed to high carbon content.

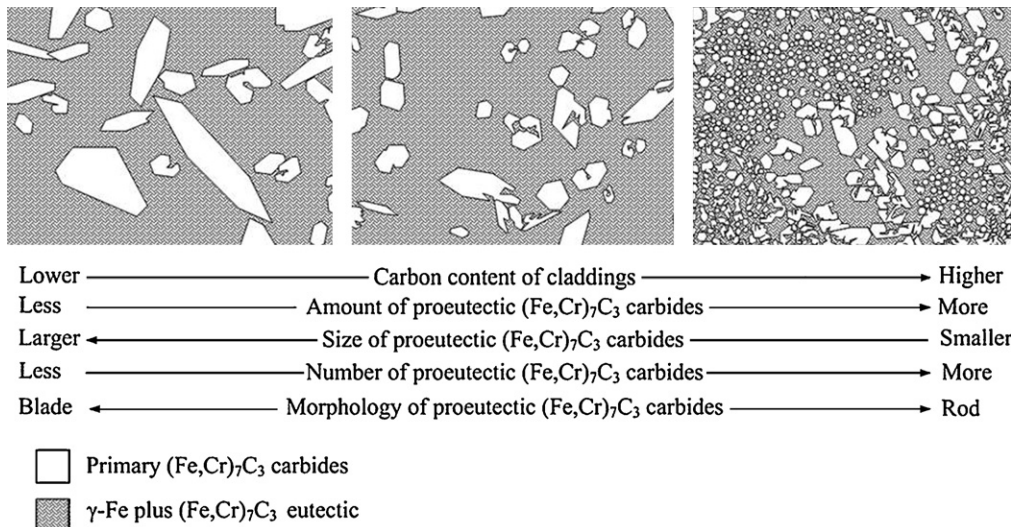


Fig. 6. Microstructural transition of hypereutectic Fe–Cr–C claddings with different C contents.

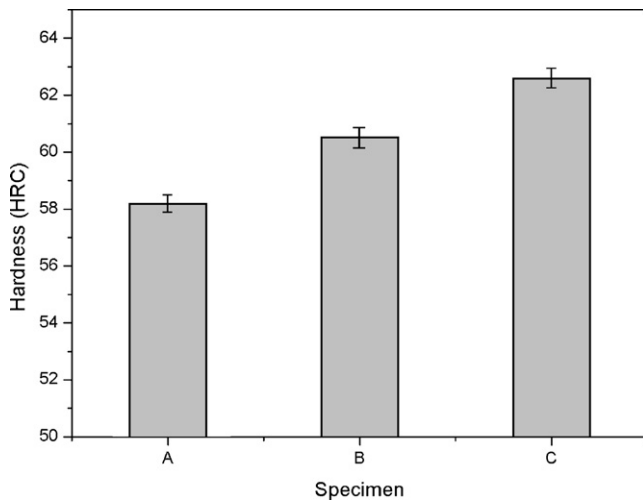


Fig. 7. The hardness of hypereutectic Fe–Cr–C claddings with different C contents.

4. Conclusions

A series of Fe–Cr–C hypereutectic claddings were fabricated by using FCAW process. With the aid of optical microscopy and scanning electron microscopy, the hypereutectic composites were found to consist of two phases: the primary $(\text{Cr,Fe})_7\text{C}_3$ and the eutectic $\gamma\text{-Fe}/(\text{Cr,Fe})_7\text{C}_3$. When the carbon content increased, the amount of proeutectic $(\text{Cr,Fe})_7\text{C}_3$ carbides increased due to the formation of primary phase caused higher undercooling. However, the reduction of their size resulted from the increment of nucleation rate

because of the higher undercooling. The morphology of proeutectic $(\text{Cr,Fe})_7\text{C}_3$ carbides transitioned from blade-like to rod-like when the carbon content of claddings. The hardness of claddings increased with the carbon content of claddings increases owing to the proeutectic $(\text{Cr,Fe})_7\text{C}_3$ carbides became more and finer.

Acknowledgement

The authors are obligated to thank the National Science Council of Taiwan, ROC for its financial support under contracts of NSC-96-2221-E-005-054.

References

- [1] C. Fan, M.C. Chen, C.M. Chang, W. Wu, *Surf. Coat. Technol.* 201 (2006) 908.
- [2] L. Lu, H. Soda, A. McLean, *Mater. Sci. Eng. A* 347 (2003) 214.
- [3] Y.C. Lin, S.W. Wang, *Tribol. Int.* 36 (2003) 1.
- [4] L.E. Svensson, B. Grefot, B. Ulander, H.K.D.H. Bhadeshia, *J. Mater. Sci.* 21 (1986) 1015.
- [5] H. Berns, A. Fischer, *Mater. Charact.* 39 (1997) 499.
- [6] H. Berns, *Wear* 254 (2003) 47.
- [7] J.D. Xing, Y.M. Gao, E.Z. Wang, C.G. Bao, *Wear* 252 (2002) 755.
- [8] S. Aso, S. Goto, Y. Komatsu, W. Hartono, *Wear* 250 (2001) 511.
- [9] P.Q. La, Q.J. Xue, W.M. Liu, *Wear* 249 (2001) 93.
- [10] C.T. Liu, J.O. Steigler, F.H. Sam Fores, *Metal Handbook*, 10th edition, The Materials Information Society, USA, 1990, p. 913.
- [11] S. Frangini, A. Masci, A.D. Bartolomeo, *Surf. Coat. Technol.* 149 (2002) 279.
- [12] P.Q. La, Q.J. Xue, W.M. Liu, S.R. Yang, *Wear* 240 (2000) 1.
- [13] G.V. Raynor, V.G. Rivlin, *Phase Equilibria in Iron Ternary Alloys*, 1st edition, The Institute of Metals, USA, 1988, p. 143.
- [14] N.R. Griffing, W.D. Forgeng, G.W. Healy, *Trans. TMS-AIME* 224 (1962) 148.
- [15] R.S. Jackson, *J. Iron Steel Inst.* 208 (1970) 163.
- [16] S. Chatterjee, T.K. Pal, *Wear* 255 (2003) 417.
- [17] G.L.F. Powell, R.A. Carlson, V. Randle, *J. Mater. Sci.* 29 (1994) 4889.
- [18] S. Atamert, H.K.D.H. Bhadeshia, *Mater. Sci. Eng. A* 130 (1990) 101.
- [19] A. Lesko, E. Navera, *Mater. Charact.* 36 (1996) 349.
- [20] O.N. Dogan, J.A. Hawk, G. Laird II, *Metall. Mater. Trans. A* 28 (1997) 1315.